fibers

MDPI

Article

Understanding Dispersion of Revolver-Type Anti-Resonant Hollow Core Fibers

Matthias Zeisberger [1], Alexander Hartung [1] and Markus A. Schmidt [1,2,3,*]

[1] Leibniz Institute of Photonic Technology, Albert-Einstein-Str. 9, 07745 Jena, Germany; matthias.zeisberger@leibniz-ipht.de (M.Z.); alexander.hartung@leibniz-ipht.de (A.H.)
[2] Otto Schott Institute of Materials Research (OSIM), Friedrich Schiller University of Jena, Fraunhoferstr. 6, 07743 Jena, Germany
[3] Abbe Center of Photonics and Faculty of Physics, Friedrich-Schiller-University Jena, Max-Wien-Platz 1, 07743 Jena, Germany
* Correspondence: markus.schmidt@leibniz-ipht.de; Tel.: +49-3641-206-140

Received: 24 August 2018; Accepted: 14 September 2018; Published: 20 September 2018

Abstract: Here, we analyze the dispersion behavior of revolver-type anti-resonant hollow core fibers, revealing that the chromatic dispersion of this type of fiber geometry is dominated by the resonances of the glass annuluses, whereas the actual arrangement of the anti-resonant microstructure has a minor impact. Based on these findings, we show that the dispersion behavior of the fundamental core mode can be approximated by that of a tube-type fiber, allowing us to derive analytic expressions for phase index, group-velocity dispersion and zero-dispersion wavelength. The resulting equations and simulations reveal that the emergence of zero group velocity dispersion in anti-resonant fibers is fundamentally associated with the adjacent annulus resonance which can be adjusted mainly via the glass thickness of the anti-resonant elements. Due to their generality and the straightforward applicability, our findings will find application in all fields addressing controlling and engineering of pulse dispersion in anti-resonant hollow core fibers.

Keywords: fiber optics; fiber design and fabrication; microstructured fibers; anti-resonant fibers

1. Introduction

Hollow core fibers (HCFs) allow for efficiently guiding light and are intensively investigated since they allow for accessing previously inaccessible fields for fiber optics or to substantially improve device performance within areas such as mid-IR gas lasers [1,2], broadband light sources [3,4], nonlinear optical effects [5], high-power pulse delivery [6], gas and liquid analytics [7,8], and pulse compression [9]. A comprehensive overview on HCFs can be found in Ref. [10]. Particular anti-resonant HCFs (ARHCFs) have recently gained substantial attraction by the Fiber Optics community since they uniquely combine low optical loss and cladding microstructures that demand only moderate fabrication efforts compared to more sophisticated fiber geometries such as photonic band gap HCFs [11–19]. The ARHCF geometry that is mostly addressed during recent times is the single-ring anti-resonant or revolver-type fiber (RTF) geometry [20–25], consisting of a finite number of thin-walled non-touching glass tubes arranged in a circle at constant azimuthal distances (Figure 1). This arrangement is mechanically stabilized by joining the individual tubes to the inner wall of a supporting capillary. As the guided field is concentrated in the core region, the supporting capillary plays a minor role for the optical properties in particular for the dispersion, and therefore we neglect it in our model. Each tube supports a well-defined number of modes (so-called annulus resonances), allowing for efficiently guiding light in the central fiber section in case these modes are not phase-matched to the core mode, i.e., core and annulus modes are anti-resonant. As a result, these glass annuluses are typically refereed

to as anti-resonant elements (ARE) [24]. The anti-resonant effect relies on the interference of the two waves reflected at the inner and outer annulus interface, leading to low-loss transmission bands that are spectrally limited by annulus resonances [26]. It is important to note that already the most generic type of ARHCF geometry—the tube-type fiber (TTF, Figure 2) geometry—qualitatively shows all key features of an ARHCF, namely strong resonances imposed by the ARE-modes and a characteristic loss evolution within the transmission bands. This approximation was utilized by several authors [27–30] to simulate complex ARHCF structures on the basis of the properties of the TTF geometry. Recent experiments involving improved designs of RTFs indicate that these types of fibers show off-resonance losses as low as 7.7 dB/km within various spectral domains [31], making it highly attractive for numerous applications.

One particular striking application that has recently attracted substantial attention is nonlinear light generation in gas-filled HCFs due to low damage thresholds, high output energy densities and the possibility for spectrally tuning the output light via pressure modification [3,4,32]. In addition to sufficiently high nonlinearities, precise control on chromatic dispersion is essential to efficiently generate supercontinua from ultrashort optical pulses [33]. Within soliton-based supercontinuum generation, the key parameter to be controlled is the group velocity dispersion (GVD), which needs to be designed such that the used ultrashort pulse does not significantly disperse over the nonlinear length and that solitons of higher orders are supported. A straightforward-to-access design parameter which is widely used throughout the ultrafast nonlinear community is the wavelength at which the GVD vanishes—the so-called zero-dispersion wavelength (ZDW)—which needs to be carefully adjusted with respect to the pump laser wavelength to allow for efficient supercontinuum generation.

In this work, we present a detailed numerical and analytical study on the dependence of important dispersion parameters on all relevant structural parameters of the RTF geometry. We found that the behaviors of phase index, GVD and ZDW are dominated by the annulus resonances (i.e., ARE wall thickness) while the actual shape of the ARE-based cladding plays only a minor role. These findings allowed us to approximate the mentioned dispersion parameters by those of the most generic type of ARHCF, the TTF geometry, which was numerically confirmed for all practically relevant situations. Using an interface reflection model to approximate the phase index of the TTF geometry, analytic expressions for the mentioned dispersion parameters were obtained, allowing us to gain fundamental insights into the dispersion behavior of the ARHCF geometry.

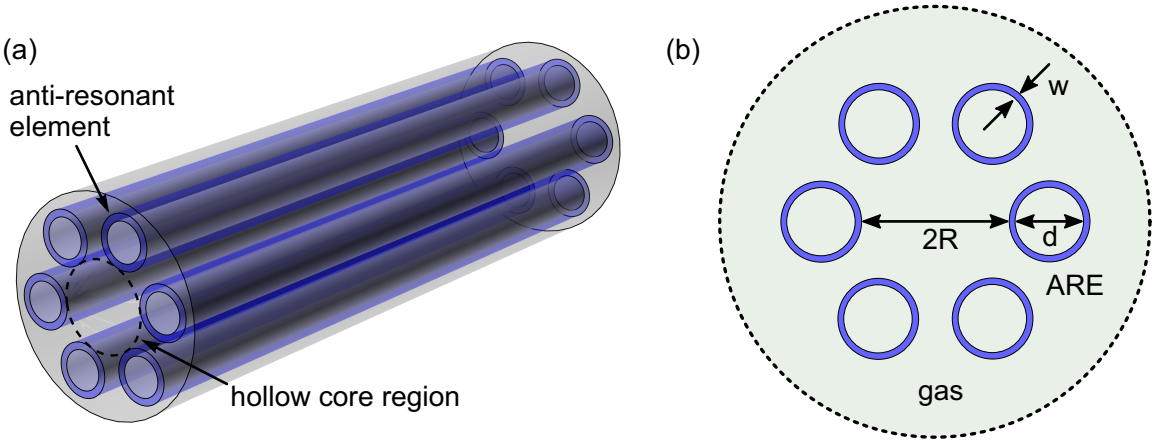

Figure 1. (**a**) illustration of the revolver-type anti-resonant hollow core fiber (RTF) geometry considered here: the fiber consists of six annulus-type anti-resonant elements (blue area) arranged around the central core region (indicted by the black dashed line); (**b**) cross section of that structure with all relevant geometric parameters. The annuluses are made from a dielectric material (typically silica glass), whereas a medium with a lower refractive index (typically gas) is located elsewhere.

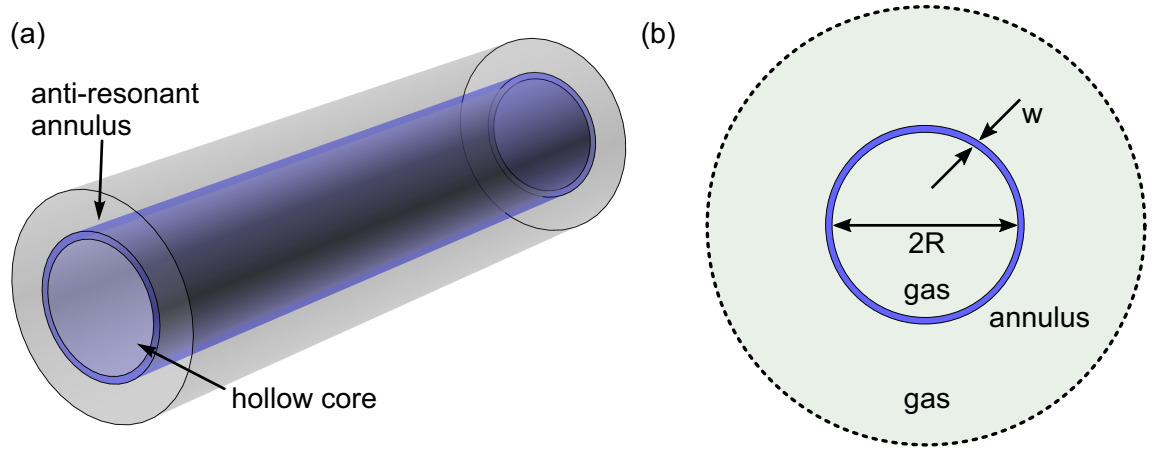

Figure 2. (**a**) sketch of the tube-type anti-resonant hollow core fiber (TTF) geometry that is used to approximate the dispersion properties of RTFs (a cross section of this geometry including the relevant parameters in shown in (**b**)). This structure is composed of a thin annulus of dielectric material containing a low index medium in the core and the most outer region.

2. Analytical Equations for GVD and ZDW

Before comparing the modal properties of RTF and TTF geometries, we would like to introduce the analytical model that allows approximating the chromatic dispersion of TTFs by an analytic expression. As shown by Marcatili et al. [34], the real part of the effective index n_{eff} (i.e., phase index) of a capillary can be expressed as $n_{eff} = 1 - a\lambda^2$ in case the capillary bore diameter is much larger than the operation wavelength λ (the parameter a depends on core radius, and mode order). The related GVD $D_\lambda = -(\lambda/c)\, d^2 n_{eff}/d\lambda^2$ (c speed of light in vacuum) only weakly depends on wavelength and, in case material dispersion is neglected, yielding an entirely analytic form $D_\lambda = 2a\lambda/c$. In contrast, the phase index of the ARHCF geometry includes an additional resonance term resulting from the interference of the waves reflected at the two glass/air interfaces, causing the GVD to strongly differ from that of a capillary particular close to the resonances [26]. For the TTF geometry (Figure 2), the spectral positions of the annulus resonances mostly depend on wall thickness w and on the refractive indices of ring and inner and outer media n_s and n_a, respectively: $\lambda_R = (2w/l)(n_s^2 - n_a^2)^{1/2}$ with $l = 1, 2, ...$ being the annulus resonance order. The same relation was reported for the RTF geometry by Uebel [24], which already indicates similarities between TTF and RTF geometries. In [26], we reported an approximate analytical model for the chromatic dispersion of the TTF geometry in case the core radius R is much larger than the operation wavelength λ (i.e., $\lambda/R \ll 1$). This model is based on a series expansion of the complex effective index with respect to λ/R up to the fourth power. For the discussion presented in this work, we are not addressing losses but chromatic dispersion only, allowing us to neglect the fourth power term that is solely related to modal attenuation and resulting in a real-valued analytic expression of the phase index (see Zeisberger for details [26]) as follows:

$$n_{eff}(\lambda) = n_a(\lambda) - AF(\lambda)\lambda^2 - BE(\lambda)C(\lambda)\lambda^3. \tag{1}$$

The parameters indicated by the capital letters are given as follows:

$$F(\lambda) = \frac{1}{n_a(\lambda)}, \quad E(\lambda) = \frac{n_s(\lambda)^2 + n_a(\lambda)^2}{n_a(\lambda)^3\sqrt{n_s(\lambda)^2 - n_a(\lambda)^2}}, \tag{2}$$

$$C(\lambda) = \cot\phi, \quad \phi = \frac{W}{\lambda}, \quad W = 2\pi w\sqrt{n_s(\lambda)^2 - n_a(\lambda)^2}, \tag{3}$$

whereas particular emphasis should be placed on the parameter C that includes a cot-function. The parameter ϕ represents the accumulated phase of the waves propagating from the outer to the inner (or vice versa) interface of the ARE. For the fundamental mode (HE_{11} mode), the constants are

$$A = \frac{j_{01}^2}{8\pi^2 R^2}, \quad B = \frac{j_{01}^2}{16\pi^3 R^3}, \quad j_{01} = 2.40. \tag{4}$$

The refractive index of the medium in the core and the outer region n_a can either be that of air or, in the context of supercontinuum generation, argon or another low index medium. It is important to note that the strand resonances are included in the factor $C(\lambda)$ and are located at the phases with the values $\phi = l\pi$ ($l = 1, 2, ...$). The corresponding GVD (i.e., dispersion parameter) is obtained by taking the second derivative of the phase index with respect to wavelength $D_\lambda = -(\lambda/c)d^2 n_{eff}/d\lambda^2$. As mentioned in the introduction section, key parameters for controlling nonlinear light generation in waveguides are GVD and ZDW, which need to be adjusted appropriately. In the following, we use Equation (1) to derive analytic expressions for both parameters. Compared to the factors λ^2, λ^3, and $C(\lambda)$, the factors $F(\lambda)$ and $E(\lambda)$ show a negligible dependence on λ, allowing us to treat them as wavelength-independent constants throughout the remaining part of the manuscript. We have checked this approximation numerically for the wavelength range 0.4–2.0 µm using the material data of argon and silica and found a deviation of less than 3% between the approximation and the exact values. The first term of Equation (1) describes the material dispersion of the core medium, which we approximate in the following by a Cauchy model that fits very well to the properties of argon for wavelengths around 1 µm (see Appendix A for details):

$$n_a(\lambda) \approx a + \frac{b}{\lambda^2}. \tag{5}$$

Here, the term b/λ^2 accounts for the material dispersion of the low index medium. In combination with Equations (2)–(5), Equation (1) yields an analytic expression for the GVD of the TTF geometry:

$$D_\lambda = -\frac{6b}{c\lambda^3} + \frac{2AF\lambda}{c} + \frac{2BE}{c}\left(\frac{W^2\cos\phi(\lambda)}{\sin^3\phi(\lambda)} + \frac{2W\lambda}{\sin^2\phi(\lambda)} + \frac{3\lambda^2\cos\phi(\lambda)}{\sin\phi(\lambda)}\right). \tag{6}$$

The first term in Equation (6) represents the contribution of the core medium (e.g., argon), the second term is the same as for a capillary, and the last term is associated with the annulus resonances. Equation (6) clearly shows that, in contrast to step-index fibers and capillaries, the TTF geometry shows a sophisticated dispersion behavior and provides more degrees of freedom for tuning GVD and ZDW. In fact, this is a result of the annulus resonances causing strong variations of $d^2 n_{eff}/d\lambda^2$ upon λ including positive and negative values particularly close to the resonances. As the main features of the fiber discussed here are related to the resonances, we derive an approximation of Equation (6) for wavelengths close to the resonances. The first step is to use the phase ϕ rather than λ as variable, i.e., λ is substituted by ϕ using Equation (3):

$$D_\lambda = -\frac{6b\phi^3}{cW^3} + \frac{2AFW}{c\phi} + \frac{2BEW^2}{c}\left(\frac{\cos\phi}{\sin^3\phi} + \frac{2}{\phi\sin^2\phi} + \frac{3\cos\phi}{\phi^2\sin\phi}\right). \tag{7}$$

Values of the phase ϕ being close to the resonances can be expressed as $\phi = l\pi - \Delta\phi$ with the off-resonance parameter $|\Delta\phi| \ll 1$. With this assumption, the following approximations can be applied

$$\frac{\cos\phi}{\sin^3\phi} \approx -\frac{1}{\Delta\phi^3}, \quad \phi \approx l\pi, \quad \phi^4 \approx l^4\pi^4, \tag{8}$$

resulting in the following approximation for the GVD of the TTF geometry:

$$D_\lambda = -\frac{6bl^3\pi^3}{cW^3} + \frac{2AFW}{cl\pi} - \frac{2BEW^2}{c}\left(\frac{1}{\Delta\phi^3} - \frac{2}{l\pi\Delta\phi^2} + \frac{3}{l^2\pi^2\Delta\phi}\right). \quad (9)$$

With this approximation, the $\Delta\phi$ value related to the ZDW can be straightforwardly obtained from the condition $D_\lambda = 0$ resulting in the following criterion for zero dispersion:

$$\Delta\phi_{ZD} = \left(\frac{BEWl\pi}{AF}\right)^{1/3}\left(1 - \frac{3bl^4\pi^4}{AFW^4}\right)^{-1/3}. \quad (10)$$

With Equations (2)–(4), we obtain the following relation for the off-resonance parameter value corresponding to the ZDW:

$$\Delta\phi_{ZD} = \left(l\pi\frac{n_s^2 + n_a^2}{n_a^2}\frac{w}{R}\right)^{1/3}\left(1 - \frac{3l^4\pi^2}{2j_{01}^2}\frac{n_a}{(n_s^2 - n_a^2)^2}\frac{b}{w^2}\frac{R^2}{w^2}\right). \quad (11)$$

The related wavelength, i.e., the ZDW can be obtained using Equation (3), leading to

$$\lambda_{ZD} = \frac{2\pi w\sqrt{n_s^2 - n_a^2}}{l\pi - \Delta\phi_{ZD}}. \quad (12)$$

It is interesting to note that the calculation above results in a positive value of $\Delta\phi$. With Equation (12), this results in values of the ZDW being larger than the related resonance wavelength, which is given by

$$\lambda_R = \frac{2w}{l}\sqrt{n_s^2 - n_a^2}. \quad (13)$$

The related anti-resonance wavelength, which is defined by the criterion $\phi = (\pi/2)(2l - 1)$ and $l = 1, 2, ...$, is given by

$$\lambda_A = \frac{4w}{2l - 1}\sqrt{n_s^2 - n_a^2}. \quad (14)$$

Equations (11) and (12) clearly suggest that the spectral position of the ZDW is associated with that of the corresponding annulus resonance, which is evident by taking the ratio between ZDW and annulus resonance wavelength of the same order $\lambda_R/\lambda_{ZD} = 1 - \Delta\phi_{ZD}/l\pi$. The relation between resonances and ZDW can also be regarded from a more general point of view. Besides the resonance regions, the fibers regarded here show approximately the same dispersion $n_{eff}(\lambda)$ as an empty capillary with $\mathrm{d}^2n_{eff}/\mathrm{d}\lambda^2 < 0$. Therefore, zero GVD, which corresponds to an inflection point $\mathrm{d}^2n_{eff}/\mathrm{d}\lambda^2 = 0$ of the dispersion, requires an additional contribution with a sufficiently large positive value of $\mathrm{d}^2n_{eff}/\mathrm{d}\lambda^2$. According to the Kramers–Kronig relation, every loss peak at a certain wavelength is related to a Lorentzian shaped dispersion with $\mathrm{d}^2n_{eff}/\mathrm{d}\lambda^2 > 0$ above the resonance wavelength.

3. Dependence of Dispersion on Number and Diameter of AREs

Compared to TTFs, the RTF geometry has two additional geometric parameters, namely the number N and the diameter d of the AREs, which might have a strong impact on chromatic dispersion. Using a finite element mode solver (FEM, COMSOL, simulation details are presented in Ref. [35]), we simulated the spectral dependence of the phase index of the fundamental HE_{11}-mode for a range of N and d values of the RTF geometry (Figure 3, $N = 5, 6, 7$; annulus 5 µm $< d <$ 25 µm) assuming a constant strand width of $w = 0.5$ µm, and material data of silica [36] and argon [37]. Remarkably, both $n_{eff}(\lambda)$ and $D_\lambda(\lambda)$ only show a weak dependence on both geometric parameters within the

investigated parameter range. In particular, the spectral evolutions of the GVDs strongly overlap across the entire bandwidth of the transmission band. Only in close proximity to the annulus resonances, differences are observed for small ARE diameters, showing that varying N and d mostly imposes a constant offset to the phase index, which is irrelevant for the GVD as it is correlated to the second derivative of n_{eff} with respect to wavelength. These results also show that the ZDW is mostly independent of N and d within practically relevant parameters' ranges, which has obvious implication on design issue related to ultrashort pulse propagation. Together with the results presented later, these findings suggest that chromatic dispersion in RTFs is dominated by the impact of the strand resonances and hardly depends on the specific properties of the actual AREs used, suggesting that the dispersion behavior of the RTF geometry is identical to that of the most generic type of anti-resonant fiber geometry, the TTF geometry. Since the core diameters of ARHCFs are substantially larger than the wavelengths considered, the above-derived analytic expressions for n_{eff} and $D_\lambda(\lambda)$ can be applied as confirmed in [26]. The resulting spectral evolutions calculated using Equations (1) and (6) (lines in Figure 3) overlap with the numerically obtained RTF results almost across the entire bandwidth of the transmission bands, whereas the match is particularly good for the GVD. An even better agreement is achieved when including a core diameter correction factor f that slightly increases the core radius R (as proposed in Ref. [24]) to account for the penetration of the core mode into the gaps between the AREs (here $f = 1.08$). It is important to note that such kind of agreement and independence on N and d is not achieved for the imaginary part of the complex effective index, which strongly depends on the microstructure used as shown in numerous works [20,22,31]. However, here we are only interested in the dispersion properties, i.e., in the real part of the effective index.

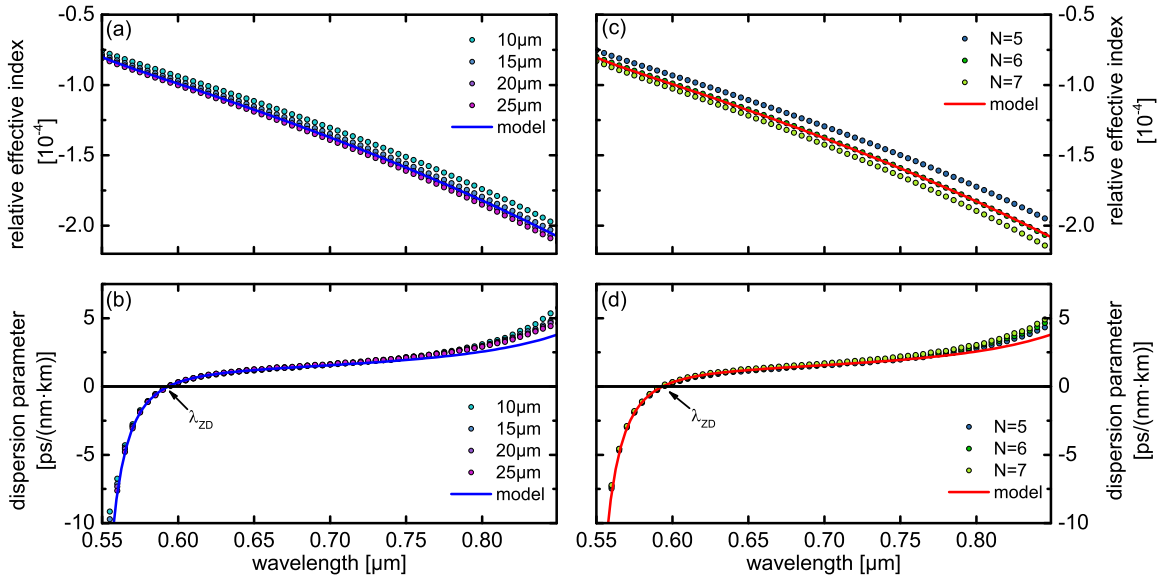

Figure 3. Spectral distributions of the real part of the effective index (top row) and of the group velocity dispersion (bottom row) for (**a**,**b**) different ARE diameters d ($N = 6$) as well as (**c**,**d**) different numbers of AREs N ($d = 20$ µm). The symbols represent the results from the numerical FEM simulations considering an RTF, whereas the lines are calculated by the analytic TTF model (Equations (1) and (6)) taking into account an effective core radius parameter of $f = 1.08$). For all data sets, we used $2R = 30$ µm, $w = 0.5$ µm, and material data of silica [36] and argon [37].

4. Dependence on the Core Radius

As a next step, we numerically investigate the dependence of phase index and GVD of the fundamental mode of the RTF geometry on a central core radius (Figure 4) while keeping the annulus parameters fixed ($w = 0.5$ µm, $d = 20$ µm, $n = 6$, refractive index distribution as for Figure 3).

As expected, the spectral distributions of both $n_{eff}(\lambda)$ and $D_\lambda(\lambda)$ strongly change in case the core dimension is modified, with the evolutions provided by our TTF model (solid lines in Figure 4) matching the numerical results particularly good within the transmission bands (dots in Figure 4). Deviations between model and numerics are only visible towards the long-wavelength side of the transmission band. The GVD-evolutions that do not include the core diameter correction factor ($f = 1$) already show excellent overlaps between TTF model and numerics (Figure 4b,d), whereas an improved match is achieved for the phase index when using $f = 1.08$ (Figure 4c,d). It is important to note that in case the strand resonances are neglected in the TTF calculations (i.e., neglecting the λ^3-term in Equation (1)), no match between model and numerics is achieved. This is, for instance, highly visible in the spectral distributions of the GVD (insets in Figure 4b,d), which never crosses the zero within the spectral domain considered here.

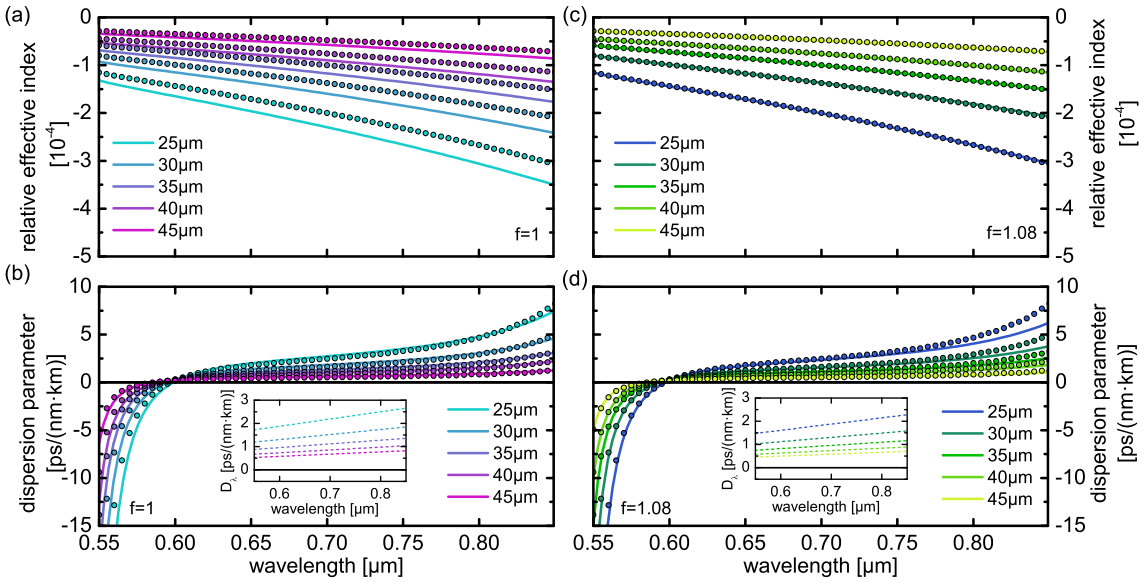

Figure 4. Spectral distributions of real part of the effective index (top row) and group velocity dispersion (bottom row) for different central core diameters of $2R = 25 - 45$ μm (**a**,**b**) excluding and (**c**,**d**) including the core diameter correction factor). The symbols represent data from the FEM simulations of the RTF geometry ($d = 20$ μm, $w = 0.5$ μm, $N = 6$), and the lines are calculated from the analytical equations for TTF (Equations (1) and (6), refractive indices defined in the caption of Figure 3). The two insets in (**b**,**d**) show the corresponding GVD distributions in case the resonance term in Equation (1) is ignored.

Due to its importance in nonlinear photonics and ultrashort pulse propagation, we take a closer look into the behavior of the ZDW in the following. Assuming the geometry considered above ($w = 0.5$ μm, $n = 6$), we have calculated the dependence of the ZDW on central core radius (Figure 5a) numerically from the FEM data of the RTF geometry, from the analytic expression of the GVD of the TTF model (Equation (7)), and by using the approximate equation for the ZDW (Equation (12)). Here, the TTF model (blue symbols in Figure 5a) accurately follows the evolution of the FEM simulations (dark blue symbols in Figure 5a), with the ZDWs matching within a spectral interval <2 nm. The analytic expression (Equation (12)) yields the correct trend, with a deviation of the ZDWs of about 8 nm. Considering that the transmission band has a spectral bandwidth of about 300 nm (see, e.g., Figure 4), this 8 nm difference yields a relative spectral deviation of about 2.5%, which yields an accuracy that is better than can be achieved in fabrication. In addition, we have also calculated the ZDW using Equations (1) and (11) within different bands, i.e., for different annulus resonance orders (Figure 5b) and plotted them together with the wavelengths of the related resonance (assuming $\Delta\phi = 0$ in Equation (12)) in Figure 5b. It is interesting to see that the ZDWs are always

located at slightly longer wavelength compared to the corresponding resonance, which is a result of the small positive values of $\Delta\phi$, i.e., $\Delta\phi > 0$ and $|\Delta\phi| \ll 1$. From the practical perspective, the most important parameter that allows for adjusting the spectral positions of annulus resonances is the respective ring width, since $\lambda_R \propto w$ (see Equation (12) in case $\Delta\phi = 0$). As a result, increasing the ring width for a constant core diameter imposes the ZDW to increase accordingly (inset of Figure 5b), again emphasizing that the emergence of a ZDW in one transmission band is a result of the presence of the annulus resonance.

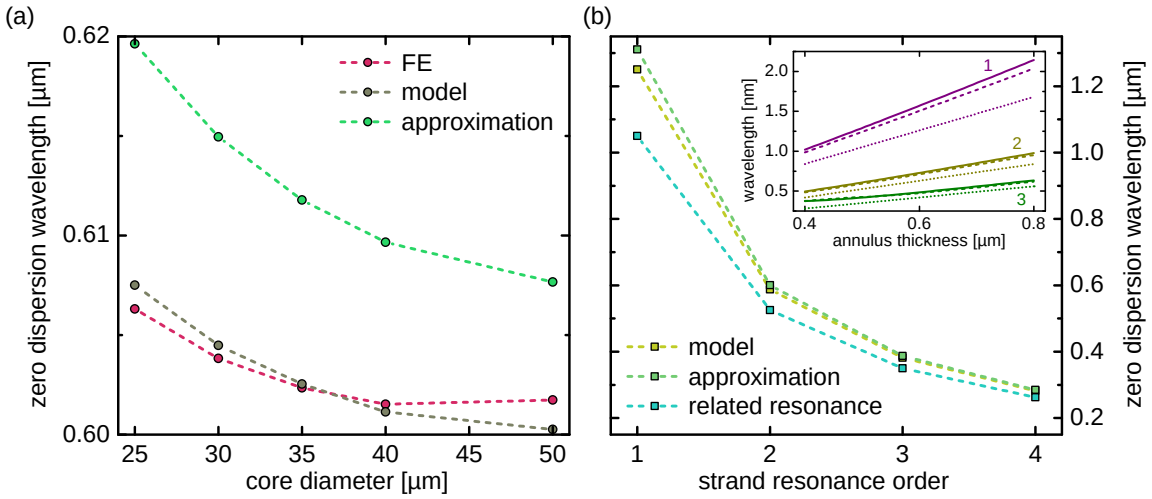

Figure 5. (**a**) dependence of the zero-dispersion wavelength on central core diameter ($w = 0.5$ µm). The three curves show the evolutions from the numerical FEM calculations (red) for $n = 6$ and $d = 20$ µm, the TTF model (Equation (6), gray) and the expression that approximate the ZDW (Equation (12), green); (**b**) ZDW vs. annulus resonance order (yellow: TTF model; green: approximate expression (Equation (12))). The cyan symbols show the related annulus resonance (according to Equation (13)). The connecting lines are only guides to the eye. The inset shows the dependence of the ZDW in case the ring thickness is changed ($2R = 50$ μm) for the three lowest resonance orders (solid lines: analytic equation (Equation (6); dashed lines: model (Equation (12)); dotted lines: corresponding resonance (Equation (13)). The colors refer to the different resonance orders (indicated by the respective numbers). Both plots assume argon and silica as gas and glass, respectively, and do not include the core diameter correction factor (i.e., $f = 1.0$).

5. Discussion

The key finding of this work is that $\mathrm{Re}(n_{eff})$ and $D_\lambda(\lambda)$ of the TTF geometry fit extremely well to the related quantities of the RTF geometry, suggesting that chromatic dispersion in ARHCF has a generic origin and is not related to a specific cladding microstructure. Here we believe that this coincidence, which is not obvious from the first view, is associated with the following reasoning: as shown in our previous work [26], the dispersion properties of the TTF geometry can by approximated to a very high degree by considering the reflection of a wave on a planar three-layer-system (e.g., here $Ar/SiO_2/Ar$) under nearly grazing incidence in the situation in which the core diameter is much larger than the operation wavelength. Here, we believe that the local fields at the surface of the individual ARE can be treated in a similar way, i.e., that the reflection process of an ARE is principally identical to that happening at a planar interface. Varying w/λ modifies the phase of the reflected wave accordingly, imposing a corresponding variation in the phase of the guided wave, i.e., in $\mathrm{Re}(n_{eff})$. This basic principle is in fact independent on the shape of the core-cladding boundary, suggesting that the dispersion behavior of the RTF geometry is dominated by the impact of the annulus resonances. The main difference between the TTF and the RTF geometry lies in local fields around the core circumference, which mostly impacts losses but not dispersion. In Ref. [29], an empirical

formula is presented that also provides an extension of the capillary dispersion [34] with a resonance term that includes empirical parameters. Equation (2) from [29] and Equation (1) from this paper can be transformed into the same mathematical form using approximations for a large core radius ($R \gg \lambda$) and a small off-resonance parameter $|\Delta\phi| \ll 1$. In this context, our results provide absolute values with analytical expressions for the strength of the resonance terms that are empirical parameters in Ref. [29]. From the practical perspective, it is important to know the modal losses in the spectral vicinity of the ZDWs. Our results show that the ZDW present in one transmission band is located in-between the anti-resonance and the related strand resonance wavelengths ($\lambda_R < \lambda_{ZD} < \lambda_A$). This is consistent with the results presented in Ref. [38] where Figure 3 shows that the ZDWs are located slightly above the resonance wavelengths, which corresponds to $0 < \Delta\phi_{ZD} \ll 1$ in terms of the work presented here. We checked all data from our FEM simulations performed in the context of this paper and found very low losses when operating close to the ZDW, whereas more sophisticated microstructures such as nested AREs yield even lower loss [23]. In the context of practical applications, the effect of geometric non-uniformity can be relevant. According to our model, the fiber dispersion can be interpreted as a combination of two effects, the dispersion of a hollow waveguide with a perfectly reflecting boundary (the first two terms in Equation (1)), and the impact of the resonances (the third term in Equation (1)). According to our model, we expect for an RTF with non-uniform wall thickness a corresponding modification of the resonances. Depending on the nature of the geometric non-uniformity, e.g., a discrete or a continuous distribution of the thickness w, we expect several discrete resonances or a broadening of the resonance, changing the overall dispersion. A detailed investigation of this effect ought to be verified by simulations, which is beyond the scope of this paper. The observed behaviors of phase index, GVD, and ZDW being dominated by the annulus resonances (i.e., ARE wall thickness), were also qualitatively found in reported experiments [39]. Even though a direct comparison to the experimental results is unfeasible due to the strand thickness variations across one fiber cross section and the additional struts in the experimentally investigated fiber, the key qualitative features (observation of one ZDW in one transmission band and the bending of the spectral distribution of the GVD in close proximity to the strand resonance) are also found experimentally, which clearly shows that the dispersion of the measured fiber is dominated by the strand resonances. Please note that the TTF-model presented here applies only to fibers with well-defined resonances that are imposed by the strands of the AREs. Photonic band gap HCFs, for instance, only exhibit a small number of transmission bands (in most cases, only one), which are separated by a comparably large spectral interval. The spectral positions of the high loss intervals cannot be described by the resonance of Equation (1) given in this work, i.e., by single strand resonances, with the consequence that the application of our model to photonic band gap HCFs is not possible.

6. Conclusions

Precise knowledge on modal dispersion is relevant for all applications involving the propagation of short pulses in optical waveguides and is particularly important within areas such as nonlinear photonics and ultrashort pulse delivery. Here, we show a detailed study of the dispersion behavior of RTFs, revealing that the resonances provided by the thin-walled annulus of the AREs surrounding the central core dominate the chromatic dispersion. Specifically, we found that the spectral distributions of phase index and GVD strongly depend on central core diameter and annulus width, whereas the modal behavior is almost independent of diameter and number of AREs used. One of the key findings of this work is that the dispersion properties (i.e., phase index and GVD) of the RTF geometry match those provided by a corresponding TTF. We derived analytic expressions for phase index and GVD that both match the corresponding features of the RTF geometry for all practically relevant situations, whereas a particular good match is obtained for the GVD. We also derived an analytic expression for the ZDW showing that each transmission band owns one ZDW, which is spectrally located in between the annulus resonance and the anti-resonance wavelengths. Moreover, the derived equations suggest that the emergence of one ZDW in one band is associated with the presence of one resonance,

i.e., that the origin of the multiple ZDWs observed in the RTF geometry is solely related to annulus resonances that are formed by the interference within the thin glass membrane. As a result of these facts, we strongly believe that both the TTF model and the analytic expressions for GVD and ZDW yield straightforward-to-use design tools that are relevant for the development of future RTFs for applications in nonlinear photonics, ultrafast light transportation and any application that demands controlling pulse dispersion in ARHCFs.

Author Contributions: M.Z. performed the analytical calculations, and A.H. the FEM simulations; M.A.S. prepared the graphics; The manuscript was written by M.Z. and M.A.S.

Funding: This research was funded by German Research Foundation (Grant SCHM2655/6-1, SCHM2655/8-1); Thuringian State Projects (2015FGI0011, 2015-0021, 2016FGR0051); European Regional Development Fund (ERDF); European Social Funds (ESF).

Conflicts of Interest: The authors declare no conflict of interest.

Appendix A

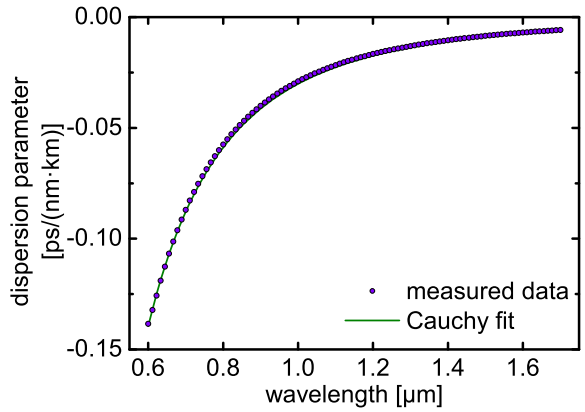

Figure A1. Spectral distribution of the GVD of argon calculated from empirical data (symbols) [37] and from Equation (A1) (line).

As shown in [37] the material dispersion of argon can be approximated by a Sellmeier expression. In case the operation wavelength is of the order of 1 µm this expression can further be approximated by first order series expansion with respect to λ^{-2} resulting in the Cauchy expression presented in Equation (5) with $a = 1.00028$ and $b = 1.507 \cdot 10^{-6}$ from which the following expression for the GVD of argon is obtained.

$$D_\lambda = -\frac{\lambda}{c}\frac{d^2 n_a}{d\lambda^2} = -\frac{6b}{c\lambda^3} \tag{A1}$$

References

1. Hassan, M.R.A.; Yu, F.; Wadsworth, W.J.; Knight, J.C. Cavity-based mid-IR fiber gas laser pumped by a diode laser. *Optica* **2016**, *3*, 218–221. [CrossRef]
2. Wang, Z.; Belardi, W.; Yu, F.; Wadsworth, W.J.; Knight, J.C. Efficient diode-pumped mid-infrared emission from acetylene-filled hollow-core fiber. *Opt. Express* **2014**, *22*, 21872–21878. [CrossRef] [PubMed]
3. Sollapur, R.; Kartashov, D.; Zürch, M.; Hoffmann, A.; Grigorova, T.; Sauer, G.; Hartung, A.; Schwuchow, A.; Bierlich, J.; Kobelke, J.; et al. Resonance-enhanced multi-octave supercontinuum generation in antiresonant hollow-core fibers. *Light Sci. Appl.* **2017**, *6*, e17124. [CrossRef] [PubMed]
4. Russell, P.S.J.; Hölzer, P.; Chang, W.; Abdolvand, A.; Travers, J.C. Hollow-core photonic crystal fibres for gas-based nonlinear optics. *Nat. Photonics* **2014**, *8*, 278–286. [CrossRef]

5. Ouzounov, D.G.; Ahmad, F.R.; Müller, D.; Venkataraman, N.; Gallagher, M.T.; Thomas, M.G.; Silcox, J.; Koch, K.W.; Gaeta, A.L. Generation of megawatt optical solitons in hollow-core photonic band-gap fibers. *Science* **2003**, *301*, 1702–1704. [CrossRef] [PubMed]
6. Jaworski, P.; Yu, F.; Carter, R.M.; Knight, J.C.; Shephard, J.D.; Hand, D.P. High energy green nanosecond and picosecond pulse delivery through a negative curvature fiber for precision micro-machining. *Opt. Express* **2015**, *23*, 8498–8506. [CrossRef] [PubMed]
7. Jin, W.; Cao, Y.; Yang, F.; Ho, H.L. Ultra-sensitive all-fibre photothermal spectroscopy with large dynamic range. *Nat. Commun.* **2015**, *6*, 6767. [CrossRef] [PubMed]
8. Nissen, M.; Doherty, B.; Hamperl, J.; Kobelke, J.; Weber, K.; Henkel, T.; Schmidt, M.A. UV Absorption Spectroscopy in Water-Filled Antiresonant Hollow Core Fibers for Pharmaceutical Detection. *Sensors* **2018**, *18*, 478. [CrossRef] [PubMed]
9. Heckl, O.H.; Saraceno, C.J.; Baer, C.R.; Südmezer, T.; Wang, Y.Y.; Cheng, Y.; Benabid, F.; Keller, U. Temporal pulse compression in a xenon-filled kagome-type hollow-core photonic crystal fiber at high average power. *Opt. Express* **2011**, *19*, 19142–19149. [CrossRef] [PubMed]
10. Harrington, J.A. *Infrared Fibers and Their Applications*; SPIE Press: Bellingham, WA, USA, 2004.
11. Cregan, R.F.; Mangan, B.J.; Knight, J.C.; Birks, T.A.; Russell, P.S.; Roberts, P.J.; Allan, D.C. Single-Mode Photonic Band Gap Guidance of Light in Air. *Science* **1999**, *285*, 1537–1539. [CrossRef] [PubMed]
12. Knight, J.C.; Broeng, J.; Birks, T.A.; Russell, P.S.J. Photonic band gap guidance in optical fibers. *Science* **1998**, *282*, 1476–1478. [CrossRef] [PubMed]
13. Benabid, F.; Roberts, P.J. Linear and nonlinear optical properties of hollow core photonic crystal fiber. *J. Mod. Opt.* **2011**, *58*, 87–124. [CrossRef]
14. Broeng, J. Photonic Crystal Fibers: A New Class of Optical Waveguides. *Opt. Fiber Technol.* **1999**, *5*, 305–330. [CrossRef]
15. Gebert, F.; Frosz, M.H.; Weiss, T.; Wan, Y.; Ermolov, A.; Joly, N.Y.; Schmidt, P.O.; Russell, P.S.J. Damage-free single-mode transmission of deep-UV light in hollow-core PCF. *Opt. Expr.* **2014**, *22*, 15388–15396. [CrossRef] [PubMed]
16. Russell, P. Photonic Crystal Fibers. *Science* **2003**, *299*, 358–362. [CrossRef] [PubMed]
17. Knight, J.C. Photonic crystal fibres. *Nature* **2003**, *424*, 847–851. [CrossRef] [PubMed]
18. Smith, C.M.; Venkataraman, N.; Gallagher, M.T.; Müller, D.; West, J.A.; Borrelli, N.F.; Allan, D.C.; Koch, K.W. Low-loss hollow-core silica/air photonic bandgap fibre. *Nature* **2003**, *424*, 657–659. [CrossRef] [PubMed]
19. Frosz, M.H.; Nold, J.; Weiss, T.; Stefani, A.; Babic, F.; Rammler, S.; Russell, P.S.J. Five-ring hollow-core photonic crystalfiber with 1.8 dB/km loss. *Opt. Lett.* **2013**, *38*, 2215–2217. [CrossRef] [PubMed]
20. Pryamikov, A.D.; Biriukov, A.S.; Kosolapov, A.F.; Plotnichenko, V.G.; Semjonov, S.L.; Dianov, E.M. Demonstration of a waveguide regime for a silica hollow-core microstructured optical fiber with a negative curvature. *Opt. Express* **2011**, *19*, 1441–1448. [CrossRef] [PubMed]
21. Kolyadin, A.N.; Kosolapov, A.F.; Pryamikov, A.D.; Biriukov, A.S.; Plotnichenko, V.G.; Dianov, E.M. Light transmission in negative curvature hollowcore fiber in extremely high material loss region. *Opt. Express* **2013**, *21*, 9514–9519. [CrossRef] [PubMed]
22. Belardi, W.; Knight, J.C. Hollow antiresonant fibers with low bending loss. *Opt. Express* **2014**, *22*, 10091–10096. [CrossRef] [PubMed]
23. Belardi, W.; Knight, J.C. Hollow antiresonant fibers with reduced attenuation. *Opt. Lett.* **2014**, *39*, 1853–1856. [CrossRef] [PubMed]
24. Uebel, P.; Günendi, M.C.; Frosz, M.H.; Ahmed, G.; Edavalath, N.N.; Menard, J.M.; Russell, P.S.J. Broadband robustly single-mode hollow-core PCF by resonant filtering of higher-order modes. *Opt. Lett.* **2016**, *41*, 1961–1964. [CrossRef] [PubMed]
25. Frosz, M.H.; Roth, P.; Günendi, M.C.; Russell, P.S.J. Analytical formulation for the bend-loss in singel-ring hollow-core photonic crystal fibers. *Photonics Res.* **2017**, *5*, 88–91. [CrossRef]
26. Zeisberger, M.; Schmidt, M.A. Analytic model for the complex effective index of leaky modes of anti-resonant single ring hollow core fibers. *Sci. Rep.* **2017**, *7*, 11761. [CrossRef] [PubMed]
27. Hayes, J.R.; Poletti, F.; Abokhamis, M.S.; Wheeler, N.V.; Baddila, N.K.; Richardson, D.J. Anti-resonant hexagram hollow core fibers. *Opt. Express* **2015**, *23*, 1289–1299. [CrossRef] [PubMed]
28. Wang, Y.; Ding, W. Confinement loss in hollow-core negative curvature fiber: A multi-layered model. *Opt. Express* **2017**, *25*, 33122–33133. [CrossRef]

29. Hasan, M.I.; Akhmediev, N.; Chang, W. Empirical formulae for the hollow-core antiresonant fibers: Dispersion and effective mode area. *J. Lightw. Technol.* **2018**, *36*, 4060–4065. [CrossRef]
30. Stawska, H.I.; Popenda, M.A.; Beres-Pawlik, E. Anti-resonant Hollow Core Fibers with Modified Shape of the Core for the Better Optical Performance in the Visible Spectral Region—A Numerical Study. *Polymers* **2018**, *10*, 899. [CrossRef]
31. Debord, B.; Amsanpally, A.; Chafer, M.; Baz, A.; Maurel, M.; Blondy, J.M.; Hugonnot, E.; Scol, F.; Vincetti, L.; Gerome, F.; et al. Ultralow transmission loss in inhibited-coupling guiding hollow fibers. *Optica* **2017**, *4*, 209–217. [CrossRef]
32. Travers, J.C.; Chang, W.; Nold, J.; Joly, N.Y.; Russell, P.S.J. Ultrafast nonlinear optics in gas-filled hollow-core photonic crystal fibers. *J. Opt. Soc. Am. B* **2011**, *28*, A11–A26. [CrossRef]
33. Dudley, J.M.; Genty, G.; Coen, S. Supercontinuum generation in photonic crystal fiber. *Rev. Mod. Phys.* **2006**, *78*, 1135–1184. [CrossRef]
34. Marcatili, E.A.J.; Schmeltzer, R.A. Hollow Metallic and Dielectric Waveguides for Long Distance Optical Transmission and Lasers. *Bell Syst. Tech. J.* **1964**, *43*, 1783–1809. [CrossRef]
35. Hartung, A.; Kobelke, J.; Schwuchow, A.; Wondraczek, K.; Bierlich, J.; Popp, J.; Frosch, T.; Schmidt, M.A. Double antiresonant hollow core fiber—Guidance in the deep ultraviolet by modified tunneling leaky modes. *Opt. Express* **2014**, *22*, 19131–19140. [CrossRef] [PubMed]
36. Palik, E.D. *Handbook of Optical Constants of Solids*; Academic Press: San Diego, CA, USA, 1998.
37. Bideau-Mehu, A.; Guern, Y.; Abjean, R.; Johannin-Gilles, A. Measurement of refractive inidces of neon, argon, krypton and xenon in the 253.7–140.4 nm wavelength range. Dispersion relations and estimated oscillator strengths of the resonance lines. *J. Quant. Spectrosc. Radiat. Transf.* **1981**, *25*, 395–402. [CrossRef]
38. Alagashev, G.K.; Pryamikov, A.D.; Kosolapov, A.F.; Kolyadin, A.N.; Lukovkin, A.Y.; Biriukov, A.S. Impact of the geometrical parameters on the optical properties of negative curvature hollow-core fibers. *Laser Phys.* **2015**, *25*, 055101. [CrossRef]
39. Grigorova, T.; Sollapur, R.; Hoffmann, A.; Schwuchow, A.; Bierlich, J.; Kobelke, J.; Schmidt, M.A.; Spielmann, C. Measurement of the dispersion of an antiresonant hollow core fiber. *IEEE Photonics J.* **2018**, *10*, 7104406. [CrossRef]